



## RESEARCH LETTER

10.1002/2013GL058999

## Key Points:

- Insolation controls changes in western African rainfall during most of the LIG
- Early LIG meltwater may have delayed the North African monsoon intensification
- Complex response of southern African rainfall with east-west contrasting trends

## Supporting Information:

- Readme
- Figure S1
- Figure S2
- Figure S3
- Figure S4
- Figure S5
- Table S1
- Table S2

## Correspondence to:

A. Govin,  
aline.govin@uni-bremen.de

## Citation:

Govin, A., V. Varma, and M. Prange (2014), Astronomically forced variations in western African rainfall (21°N–20°S) during the Last Interglacial period, *Geophys. Res. Lett.*, 41, 2117–2125, doi:10.1002/2013GL058999.

Received 9 DEC 2013

Accepted 18 FEB 2014

Accepted article online 19 FEB 2014

Published online 17 MAR 2014

## Astronomically forced variations in western African rainfall (21°N–20°S) during the Last Interglacial period

Aline Govin<sup>1</sup>, Vidya Varma<sup>1</sup>, and Matthias Prange<sup>1</sup><sup>1</sup>MARUM—Center for Marine Environmental Sciences, University of Bremen, Bremen, Germany

**Abstract** This study documents the long-term evolution of western African precipitation during the Last Interglacial (LIG). We compare geochemical records obtained on nine sediment cores from the western African margin to a transient simulation (130–115 ka) performed with an ocean-atmosphere general circulation model and insolation as sole forcing. Good agreement between proxy records and model outputs indicates that long-term changes in western African precipitation largely responded to insolation variations during most of the LIG. After an early LIG dry phase (related to high-latitude iceberg melting or dating uncertainties), boreal summer insolation controlled the intensification of the North African monsoon between 127 and 122 ka, perhaps facilitating human migrations out of Africa. Equatorial African rainfall slightly increased throughout the LIG in response to increasing annual insolation. East-west contrasting rainfall evolutions at 10–20°S illustrate the complex southern African response, in contrast to more direct responses of North and equatorial western Africa, to insolation forcing.

### 1. Introduction

The evolution of African climate throughout the Last Interglacial period (LIG, ~129–116 ka, 1 ka = 1000 years before present) is of particular interest in the context of human dispersal out of Africa [Walter *et al.*, 2000]. It has been suggested that high boreal summer insolation at the beginning of the LIG strengthened the NW African monsoon [e.g., Castañeda *et al.*, 2009] and led to the development of an extensive interconnected hydrological system across North Africa [Drake *et al.*, 2011]. These waterways facilitated the dispersal of modern humans across the “green Sahara” and out of Africa [e.g., Osborne *et al.*, 2008; Armitage *et al.*, 2011]. The timing of such human migrations remains relatively vague, ranging between 135 and 110 ka [Walter *et al.*, 2000; Osborne *et al.*, 2008; Castañeda *et al.*, 2009; Armitage *et al.*, 2011].

Because of the lack of dedicated studies, our understanding of African climate evolution during the LIG is limited. Long low-resolution records suggest wet LIG conditions in northern Africa [e.g., Prell and Kutzbach, 1987; Castañeda *et al.*, 2009] and in equatorial Africa [Gingele *et al.*, 1998] and arid conditions in southern Africa [Partridge *et al.*, 1997]. Although extensively investigated during the Holocene [e.g., Claussen *et al.*, 2013], the response of the North African monsoon to orbital changes has been the focus of very few time-slice studies during the LIG [Braconnot *et al.*, 2008] and has not been investigated throughout the transition. Whereas central and southern Africa reveal a complex picture of rainfall changes during the Holocene [Burrough and Thomas, 2013], the evolution and drivers of precipitation changes in these regions are unknown during the LIG. Therefore, the scarcity of African records that cover the LIG has hampered investigation of the spatiotemporal response of African climate to the large seasonal insolation forcing during the LIG.

This study aims to (1) document the detailed LIG spatiotemporal evolution of western African precipitation and (2) assess whether astronomical forcing is responsible for the LIG hydroclimatic evolution. We hence compare high-resolution geochemical records of nine marine sediment cores located along the western African margin (21°N–20°S) to the results of a transient climate simulation (130–115 ka) performed with a fully coupled ocean-atmosphere general circulation model and with insolation changes as sole forcing. We show that long-term changes in western African precipitation respond to insolation variations during most of the LIG, with a much more complex rainfall response in southern Africa than in North and equatorial western Africa. Persistent melting of northern ice sheets may also have contributed to a delayed NW African monsoon intensification during the early part of the LIG.

## 2. Material and Methods

### 2.1. Paleoclimate Records

Multisite studies using the same paleotracer bring a comprehensive view of past African climate changes [Collins *et al.*, 2011]. Nine marine sediment cores from the western African margin (Table S1 in the supporting information) were geochemically analyzed to reconstruct past changes in African hydroclimatic conditions. Located between 21°N and 20°S, they cover the modern range of the African rainbelt's seasonal oscillations. Situated a few kilometers away from the African coast, the sites receive large amounts of terrigenous material (see Figure S1 for main source regions). All sites receive input from nearby rivers, in particular from the Senegal, Niger, and Congo Rivers. The northernmost sites (9–21°N) receive large quantities of Saharan-Sahelian dust [e.g., Engelstaedter *et al.*, 2006], whereas the input of eolian material is limited at 3°N and 7°S [Stuut *et al.*, 2005]. Southernmost sites (12–20°S) mainly receive wind-blown dust from the Namib and Kalahari deserts in southern Africa [e.g., Prospero *et al.*, 2002] (Figure S1).

Our present study focuses on the interval of the LIG. We infer past changes in western African hydroclimatic conditions from the commonly used Al/Si ratio [e.g., Mulitza *et al.*, 2008; Govin *et al.*, 2012b; Collins *et al.*, 2013]. High Al/Si values reflect increased input of highly weathered material (rich in kaolinite) derived from tropical humid regions [e.g., Govin *et al.*, 2012b]. The Al/Si ratio also depends on the grain size of terrigenous material, with high Al/Si values reflecting high input of fluvial fine-grained (kaolinite-rich) material [Mulitza *et al.*, 2008]. The similar water depth range of sediment cores considered here (1900–3500 m, Table S1) indicates similar grain size fractionation associated with transport distance between cores [Collins *et al.*, 2013]. Therefore, downcore Al/Si variations reflect past changes in terrestrial climatic conditions in the regions where terrigenous material originates, regardless of the mode of transport [e.g., Govin *et al.*, 2012b]. Figure S1 shows estimated source areas of terrigenous material delivered to core sites, i.e., main geographic regions for which past climatic variations are reconstructed from the Al/Si ratio.

Major element variations were obtained from X-ray fluorescence core scanning and calibrated against elemental concentrations measured on powdered sediment samples [Weltje and Tjallingii, 2008]. LIG records are of high resolution, ranging on average between 0.3 and 0.6 ka in cores A–F, and 0.5 and 0.9 ka in cores G–I. The Al/Si ratio was corrected for downcore changes in biogenic opal in cores F–H (3°N–12°S) characterized by high biogenic opal contents [Schneider *et al.*, 1997; Holtvoeth *et al.*, 2005]. Age models are based on the synchronization of benthic foraminiferal oxygen stable isotope ( $\delta^{18}\text{O}$ ) records to the North Atlantic reference core MD95-2042 [Shackleton *et al.*, 2002] (Figure S2). We also used the benthic  $\delta^{13}\text{C}$  records to improve the stratigraphy of cores where *Cibicides* data are available (not shown). Core MD95-2042 records were transferred on the recent AICC2012 ice core chronology [Govin *et al.*, 2013], using the methodology described in details for the LIG in Govin *et al.* [2012a]. This approach produces age models that fully agree with the LR04 stack [Lisiecki and Raymo, 2005] (Figure S2), but it circumvents the low resolution of LR04 and its problematic combination of benthic  $\delta^{18}\text{O}$  records from different oceanic basins and water depths, when offsets of several thousand years are known to occur across water masses during deglaciations [Lisiecki and Raymo, 2009]. We estimated dating uncertainties associated with defined tie points (see Table S2). To propagate these errors, we applied to all cores a Monte Carlo analysis performed with 1000 age model simulations. For every iteration, we (1) randomly determined the age of every tie point within the range of combined dating uncertainties documented in Table S2 (last column), (2) checked for potential age reversals and discarded the iteration if it is the case, and (3) assigned an age to every depth for which Al/Si data are available, by linear interpolation (i.e., constant sedimentation rate) between tie points as defined in step 1. This procedure produces 1000 slightly different ages for every downcore Al/Si value. We hence calculated median ages and associated percentiles to produce five different age models per core: the main age model obtained from median ages, two obtained from the sixteenth and 84th percentiles to define a nonparametric 1 $\sigma$  confidence interval, and two from the 2.5th and 97.5th percentiles to define the 2 $\sigma$  confidence interval. In this approach, we neglect Al/Si measurement errors relative to larger dating uncertainties, which explains the “flat horizontal aspect” of confidence intervals (Figure 1).

### 2.2. Model Simulations

Transient LIG simulations have been carried out using the comprehensive global climate model CCSM3 (Community Climate System Model version 3). National Center for Atmospheric Research's CCSM3 is a state-of-the-art fully coupled model, composed of four separate components representing atmosphere,

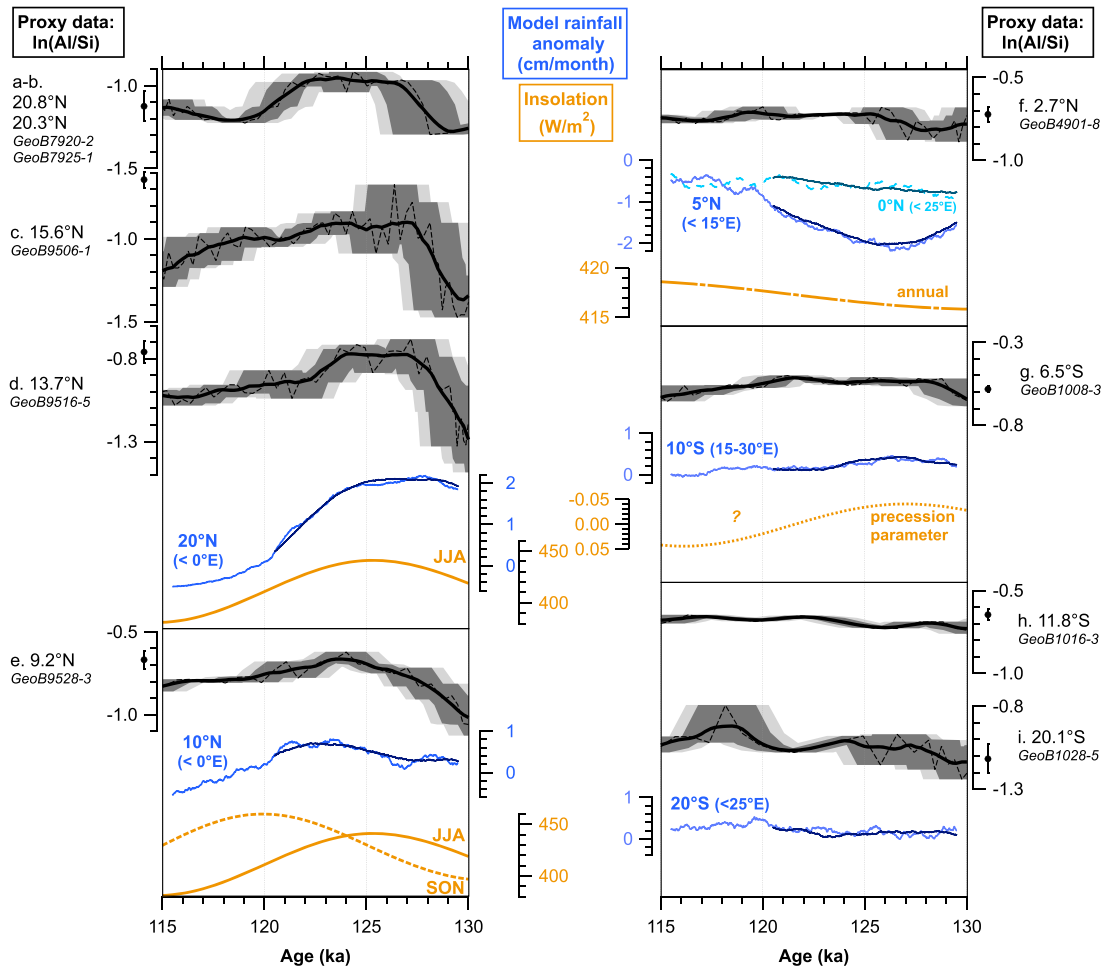


**Figure 1.** Evolution of proxy data (in grey), model rainfall (in blue), and insolation (in orange) variations between 130 and 115 ka. Used as an indicator for past hydroclimatic conditions in western Africa [Govin *et al.*, 2012b], the Al/Si log ratio is plotted for all marine sediment cores at (a and b) 21°N, (c) 16°N, (d) 14°N, (e) 9°N, (f) 3°N, (g) 7°S, (h) 12°S, and (i) 20°S. Dashed lines show original Al/Si data plotted on the age model produced with median ages during the Monte Carlo analysis (see text). The thick black line is a 2 ka smoothing (after resampling every 0.25 ka) of these Al/Si data. Grey shaded areas mark nonparametric 1 $\sigma$  (sixteenth and 84th percentiles, dark grey) and 2 $\sigma$  (2.5th and 97.5th percentiles, light grey) confidence intervals of Monte Carlo iterations (see text). For comparison, black dots along the Y axes show the ln(Al/Si) values ( $\pm 1\sigma$ ) averaged over the period 8–10 ka (boreal summer insolation maximum of the present interglacial). The evolution of zonally averaged annual mean precipitation simulated in western Africa is shown in blue for specific latitudinal bands (see Figure S1): 20°N for Figures 1a–1d, 10°N for Figure 1e, 5°N for Figure 1f, and 0° (dashed line), 10°S for Figure 1g, and 20°S for Figures 1h and 1i. Time series of rainfall anomalies (relative to the preindustrial control simulation) shown for the accelerated (light blue) and nonaccelerated (dark blue) transient simulations were smoothed with a 1000 orbital year (corresponding to 100 model integration years in the accelerated run) boxcar filter. Insolation variations at 0° [Laskar *et al.*, 2004] are shown in orange: seasonal variations in June–July–August (JJA) in Figures 1a–1e and September–October–November (SON) in Figure 1e, annual insolation in Figure 1f, and changes in the precession parameter in Figure 1g [Laskar *et al.*, 2004]. The question mark in the precession parameter panel highlights that precession-induced JJA insolation may not be the sole driver of the 10°S rainfall evolution (see text for details).

ocean, land, and sea ice [Collins *et al.*, 2006]. The resolution used in our simulations is given by T31 (3.75° transform grid) in the atmosphere (26 layers), whereas the ocean has a nominal resolution of 3° (like the sea ice component) with refined meridional resolution (0.9°) around the equator and 25 vertical levels [Yeager *et al.*, 2006].

The transient simulations start from a quasi-equilibrated 130 ka time-slice run, which in turn was branched off from a 9 ka simulation [Varma *et al.*, 2012] and integrated for another 400 years. Two transient runs were carried out: one with orbital acceleration [Lorenz and Lohmann, 2004] of factor 10 (130–115 ka) and a shorter one without acceleration (130–120 ka). In both runs, only insolation varies, whereas greenhouse gas concentrations are fixed to the mean values of the period 130–120 ka (i.e., 272 ppmv for CO<sub>2</sub>, 622 ppbv for CH<sub>4</sub>, and 259 ppbv for N<sub>2</sub>O). Preindustrial ozone and aerosol fields are applied [Otto-Bliesner *et al.*, 2006]. Fixed modern distributions of continental ice sheets and vegetation are used throughout the simulations. Although vegetation composition changed in the Sahel region during the LIG [Castañeda *et al.*, 2009], unpublished

early to mid-Holocene simulations performed with fixed and interactive vegetation indicate that vegetation changes alter the magnitude (up to 25%) but not the sign of North African precipitation variations. Because the Al/Si ratio is not a quantitative proxy of rainfall amount, our model-data comparison focuses on African precipitation evolution trends throughout the LIG. The assumption of fixed vegetation in this study has, therefore, limited effects on our model-data comparison. For the model-data comparison, we use the longer accelerated transient simulation, whereas the shorter unaccelerated run is required to validate the acceleration technique. The accelerated run has previously been analyzed in terms of LIG temperature evolution [Bakker *et al.*, 2013].

### 3. Results

#### 3.1. Proxy Records

The North African cores (21–9°N) exhibit an increase in Al/Si values during the early LIG until  $\sim 127.5 \pm 2$  ka at 21–14°N and  $124 \pm 1$  ka at 9°N (Figure 1). High Al/Si values between  $\sim 127$  and 122 ka suggest humid North African conditions during peak interglacial warmth (Figures 1a–1e). Consecutively, decreasing Al/Si values between  $\sim 122$  and 115 ka reveal a gradual drying of North African climate during the late LIG and the early glacial inception (Figures 1a–1e). The cores at 3°N and 7°S exhibit high Al/Si values throughout the studied interval (Figures 1f and 1g), indicating relatively constant and wet conditions within the core catchments. The 3°N core exhibits slightly increasing Al/Si values between 128 and 124 ka followed by relatively stable values (Figure 1f), whereas slightly decreasing Al/Si values are recorded at 7°S between 121 and 115 ka (Figure 1g). The southernmost cores at 12°S and 21°S exhibit varying Al/Si values with no clear emerging trend throughout the studied interval (Figure 1h and 1i). This feature indicates no large change in terrestrial hydroclimatic conditions in the southern part of Africa during the LIG. Our LIG data also reveal Al/Si values that are within the range of values recorded during the early Holocene (10–8 ka), in particular in northern Africa (Figure 1).

Finally, Al/Si variations exhibit high similarities to Al/K variations in all cores during the LIG, as well as to available indicators of African hydroclimatic conditions that are independent of sedimentary geochemical compositions (see Figure S3 for a detailed discussion). This result supports the use of the Al/Si ratio as a tracer of African hydroclimatic conditions in regions where terrigenous material specifically originates (Figure S1).

#### 3.2. Model Results

The general long-term spatiotemporal evolution of western African rainfall between 130 and 115 ka is visualized by the first empirical orthogonal function (EOF) of annual precipitation (Figures 2a and 2b). This mode explains 76% of the variance (Figures 2a and 2b). Whereas northern Africa and coastal regions of Namibia and Angola exhibit decreasing rainfall evolutions, opposite precipitation trends are observed in equatorial and eastern southern Africa (Figure 2). Southern Africa (10–25°S) hence exhibits a clear east-west rainfall contrast, with an overall decrease in rainfall along the coast of Namibia and Angola and an increase in precipitation further inland, east of  $\sim 20^\circ\text{E}$  (Figures 2a and 2b). The strongest precipitation changes take place in North Africa between 10°N and 20°N (Figure 2a) and between 124 and 117 ka (Figure 2b).

Changes in African rainfall are closely linked to variations in sea level pressure (SLP, see section 4). The first EOF of annual mean SLP (Figures 2c and 2d) explains 85% of the variance. An increase in SLP between 127 and 116 ka is observed in both subtropical African regions (North Africa to the north of 20°N and southern Africa to the south of 10°S), whereas a decrease is simulated in North and Central Africa between 20°N and  $\sim 10^\circ\text{S}$  (Figures 2c and 2d).

### 4. Discussion

In order to assess whether the reconstructed LIG variations in African hydroclimatic conditions are consistent with astronomically forced changes in precipitation, we compare the Al/Si proxy records with the transient model simulation driven by orbital forcing only. Although we estimated the main source regions delivering terrigenous material to the coring sites, the precise extent of catchment areas cannot be properly determined. We hence consider time series of zonally averaged western African rainfall for six characteristic latitudes in the model (Figure 1, in blue), which agree with approximate source regions identified for each core (Figure S1). How well the model and proxy data agree throughout the LIG is investigated using standardized data in Figure S4.

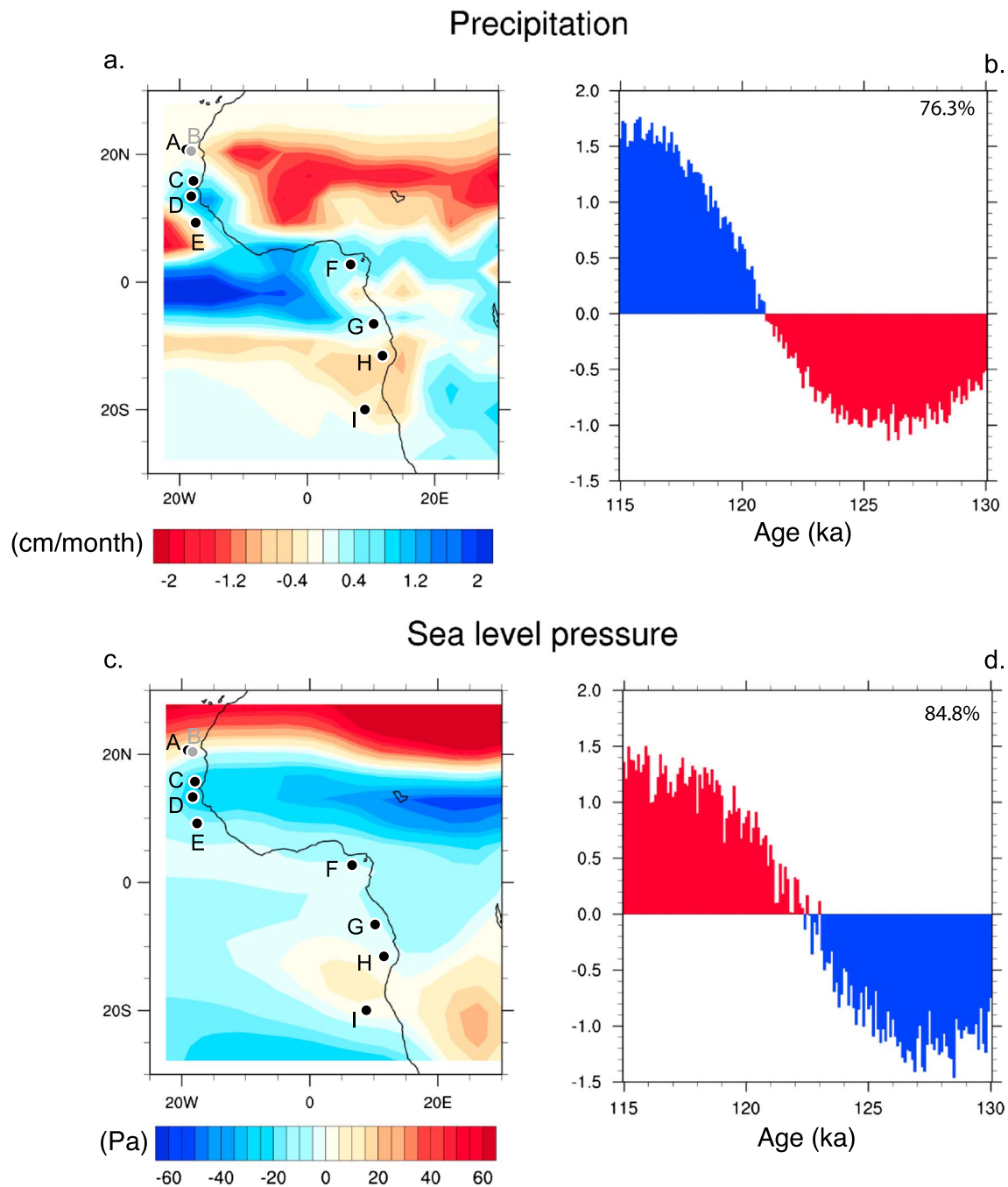


**Figure 2.** (a and c) Spatial distribution and (b and d) time series of the first empirical orthogonal function (EOF) of annual mean precipitation in Figures 2a and 2b and sea level pressure in Figures 2c and 2d simulated for Africa for the period 130 to 115 ka. Note the inverted color scales in both panels. The EOF analysis was performed on serial 100 orbital year (corresponding to 10 model integration years) mean values of the accelerated transient simulation. (Figure 1 shows that the long-term evolution of African precipitation is highly similar in the accelerated and nonaccelerated simulations.) The time series are standardized, and the EOF maps are obtained by regressing the precipitation/sea level pressure data onto the corresponding standardized leading principal component time series [von Storch and Zwiers, 1999]. Figures 2a (spatial distribution) and 2b (time series) need to be combined to deduce the temporal evolution of precipitation in specific African regions from 130 to 115 ka. The evolution from negative to positive principal component time series values from ~126 to 115 ka (see Figure 2b) indicates (1) rainfall increase in regions characterized by positive anomalies in Figure 2a (e.g., southeastern Africa) and (2) rainfall decrease in regions characterized by negative anomalies in Figure 2a (e.g., North Africa) throughout this time interval. The same type of reasoning applies to Figures 2c and 2d to deduce the temporal sea level pressure evolution in different regions of Africa from 130 to 115 ka.

Orbitally driven changes in annual precipitation simulated at 20°N indicate high rainfall in North Africa between 130 and 124 ka and a substantial rainfall decrease between 124 and 115 ka (with the strongest reduction taking place between 124 and 119 ka, Figures 1a–1d). This decrease in annual rainfall at 20°N is controlled by the gradual reduction in boreal summer (June–July–August, JJA) insolation (Figures 1a–1d), which progressively reduces the strong heating of North Africa, enhances SLP in North Africa (Figure 2), and weakens the NW African monsoonal rainfall. Standardized data indicate similar LIG evolutions, within dating uncertainties, of North African precipitation simulated by the climate model and Al/Si records obtained at 14–21°N, in particular between 127 and 115 ka (Figure S4). This result supports the well-known control of boreal summer insolation on the North African monsoon [e.g., *Prell and Kutzbach, 1987; Tjallingii et al., 2008*] and indicates that JJA insolation variations control the long-term evolution of North African precipitation during most of the LIG period. It is, however, not clear whether orbital forcing is the sole driver of North African precipitation at the beginning of the LIG. Whereas the astronomically forced model simulation shows enhanced North African rainfall from 130 ka on (Figures 1a–1d), NW African records (14–21°N, Figures 1a–1d) tend to indicate lower Al/Si values between 130 and ~127.5 ka than during the period of intensified North African monsoon between ~127 and 122 ka. Severe NW African drought events are observed during the Younger Dryas and Heinrich stadials of the last 60 ka [e.g., *Street-Perrott and Perrott, 1990; Mulitza et al., 2008; Collins et al., 2013*]. Similarly, persistent iceberg melting and reduced deep ocean circulation documented in the North Atlantic and Nordic Seas during the early LIG [e.g., *Govin et al., 2012a*] could induce relatively dry North African conditions during the early LIG and delay the LIG intensification of the North African monsoon. However, relatively large dating uncertainties during the LIG make the starting date of high Al/Si values uncertain in proxy records (Figures 1a–1d). Therefore, the time lag between the beginning of intensified North African precipitation simulated from 130 ka on and high Al/Si values (indicative of enhanced North African rainfall) recorded at  $\sim 127.5 \pm 2$  ka ( $1\sigma$ ) is close to dating uncertainties (Figures S4a–S4d). Proxy records with reduced dating errors would thus be required to verify whether the delay in North African monsoon intensification is a robust feature of the early LIG climate or related to chronological uncertainties.

The situation is slightly different at 10°N, where the maximum in annual rainfall occurs later (between 126 and 121 ka, Figure 1e) in the model simulation than at 20°N. This pattern agrees very well, within dating errors, with Al/Si variations recorded at 9°N (see standardized data in Figure S4e), as well as with existing studies from this latitude [*Castañeda et al., 2009*]. The decrease in JJA rainfall due to decreasing JJA insolation (Figure 1e) controls the reduction in annual rainfall simulated at 10°N at the end of the LIG (Figure S5). We also observe at 10°N an increase in annual rainfall between 130 and 122 ka that contrasts to the high annual rainfall simulated at 20°N between 130 and 124 ka (Figure 1). Whereas 10°N JJA rainfall remains high between 130 and 124 ka, the amplitude of the increase in September–October–November (SON) rainfall between 130 and 121 ka is larger than that of the simultaneous decrease in March–April–May rainfall (Figure S5a). The increase in 10°N annual rainfall between 130 and 122 ka hence derives from the SON rainfall increase that responds to increasing SON insolation (Figure 1e). High SON contribution to annual rainfall at 10°N during the LIG agrees with the modern climatology where both SON and JJA rainfall contribute to the rainy season (Figure S5a). In contrast to the situation at 20°N, the model results indicate that astronomical forcing contributes to the late LIG rainfall maximum recorded at 9°N (Figure 1e). Dating uncertainties in proxy records are too high to allow conclusions on the influence of meltwater input on western African climate at 10°N during the early LIG.

In equatorial regions, the model simulates an increase in annual rainfall between 127 and 117 ka at 5°N and slight increase in annual rainfall from 130 to 120 ka (followed by relatively constant precipitation values until 115 ka) at 0°N (Figure 1f). The 3°N core also exhibits increasing Al/Si values during the LIG (mainly between 128 and 124 ka, Figure 1f). Although terrigenous material delivered at the 3°N site derives from mountainous regions around 5°N where the Benue and Sanaga Rivers originate (Figure S1), standardized data indicate better agreement of the 3°N proxy record with the LIG rainfall evolution simulated at the equator than at 5°N (Figure S4f). This result illustrates the limitation of our model-data comparison with the relatively coarse T31 (approximately 3.75° resolution) model resolution. Nevertheless, both modeled rainfall time series indicate that seasonal rainfall variations in equatorial Africa respond to seasonal insolation changes, which largely cancel each other in the annual mean (Figure S5b). Therefore, the increase in annual rainfall simulated in equatorial regions during the LIG follows the increase in annual mean equatorial insolation (Figures 1f and S5b) driven by the obliquity decrease [*Loutre et al., 2004*]. This result confirms that precession may not be the sole orbital parameter controlling past African precipitation changes [e.g., *Tuenter et al., 2003*].

At 10°S, the model simulates a decrease in annual rainfall after 126 ka, which mimics the decrease in Al/Si values recorded at 7°S between 121 and 115 ka (Figure 1g). Larger than dating uncertainties (Figure S4g), timing mismatches between model and proxy data are difficult to explain. They may be related to the difficulty of identifying the exact provenance of terrigenous material within the large Congo Basin (Figure S1). Nevertheless, this progressive drying is consistent with increasing SLP simulated over southern Africa during the LIG (Figures 2c and 2d), which reduces the westerly inflow of moist Atlantic air onto the continent. The model simulation indicates that all seasons contribute the annual precipitation evolution at 10°S (Figure S5c). In particular, although very limited in southern tropical Africa around 10°S today, dry-season JJA rainfall is substantially enhanced between 130 and 121 ka (Figure S5c). This situation at 10°S contrasts with the North African monsoonal system where wet-season rainfall dominates the annual rainfall evolution (Figure S5a). It is difficult to identify the drivers of the annual rainfall decrease observed in tropical southern Africa during the LIG (Figure 1g). Paleoreconstructions suggest strong links between precipitation changes over the Congo Basin and boreal summer insolation (precession parameter) over the last 200 ka, with enhanced rainfall and expansions of the rain forest during periods of high JJA insolation [e.g., *Gingele et al.*, 1998; *Dupont*, 2009]. Enhancement of JJA rainfall simulated at 10°S during high JJA insolation (Figure S5c) would reduce the dry-season length and favor rain forest expansion [*Maley*, 1991]. However, the decrease in dry-season JJA rainfall simulated across the LIG is largely compensated by the increase in wet-season (DJF) rainfall (Figure S5c). The decrease in annual rainfall at 10°S may result from the combination of spring and autumn rainfall evolutions (Figure S5c), rather than from the increase in JJA insolation (precession parameter) as suggested so far by available data. Our results illustrate here the complex response of southern African climate and rainfall to insolation changes [e.g., *Burrough and Thomas*, 2013].

Little change in annual rainfall is simulated at 20°S between 130 and 115 ka (Figures 1h and 1i). Standardized data indicate a good agreement, within dating uncertainties, of the model evolution with our proxy records at 12–20°S that exhibit varying Al/Si values with no clear emerging trend throughout the LIG (Figures S4h and S4i). The model simulation shows strong east-west contrasting rainfall trends over southern Africa (Figures 2a and 2b). The reduction in annual precipitation simulated along coastal regions mimics the rainfall evolution at 10°S (Figures 2a and 2b) as already discussed in the previous paragraph. In contrast, the intensification of precipitation simulated over inland southern Africa during the LIG (Figures 2a and 2b) agrees with continental records from South Africa, which indicate enhanced South African summer rainfall during periods of high austral summer insolation [*Partridge et al.*, 1997]. This result suggests that increasing austral summer insolation during the LIG controls the intensification of annual rainfall simulated over inland southern Africa (Figures 2a and 2b). However, averaging precipitation changes over a large zonal band (Figure S1) leads to a cancelation of the east-west rainfall trends and explains why few hydroclimatic changes are observed in southern Africa (Figures 1h and 1i). Similar precipitation evolutions indicated for the southern African region by model results and proxy records (Figure S4h and S4i) confirm that the marine sites receive terrigenous material from a wide area and integrate climate changes over a large continental region. Similar contrasting east-west rainfall trends in southern Africa as during the LIG are also observed during the Holocene. Whereas a progressive decrease in regional humidity is recorded in northwestern Namibia across the Holocene [e.g., *Chase et al.*, 2010], marine sediments tracing precipitation changes over the Zambezi basin indicate a gradual increase in southeastern African rainfall after 8 ka [*Schefuß et al.*, 2011]. These observations suggest a complex response of southern African climate to orbital forcing, with east-west contrasting rainfall trends that may be a recurring feature of interglacial climate evolutions.

## 5. Conclusions

To elucidate the long-term evolution of western African precipitation during the LIG, we compared geochemical records from the western African margin with results from a transient LIG simulation where insolation is the sole forcing. The generally good agreement between proxy records and model output indicates that astronomical forcing is the primary driver of reconstructed long-term changes in western African hydroclimate during most of the LIG.

Intensification of the North African monsoon during the LIG led to the development of an extensive interconnected hydrological system in northern Africa that facilitated human dispersals across the Sahara and out of Africa [e.g., *Osborne et al.*, 2008; *Armitage et al.*, 2011; *Drake et al.*, 2011]. These migrations may have

occurred during times of strongest North African rainfall, i.e., between  $127 \pm 2$  ka and  $122 \pm 2$  ka ( $1\sigma$ ) according to our results. Persistent meltwater and weakened deep North Atlantic circulation during the early LIG may have delayed the orbitally driven intensification of the North African monsoon, but large dating uncertainties in proxy records prevent firm conclusions as to the exact timing of the meltwater input. Both proxy records and model simulations also suggest a gradual drying of the North African climate rather than an abrupt termination of the LIG humid period. Finally, opposite east-west rainfall evolutions at  $10$ – $20^\circ\text{S}$  (drying in western coastal areas, wetting in inland regions) reflect the complexity of southern African climate variability in response to insolation forcing.

### Acknowledgments

We acknowledge the Geoscience Department and GeoB Core Repository at MARUM–University of Bremen for supplying sediment samples. This research used data acquired at the XRF Core Scanner Lab from MARUM–University of Bremen. The sediment core data reported in this paper are archived in Pangaea ([www.pangaea.de](http://www.pangaea.de)). CCSM3 simulations were performed on the SGI Altix supercomputer of the Norddeutscher Verbund fuer Hoch- und Hochleistungsrechnen (HLRN). This work was funded through the DFG Research Center/Cluster of Excellence “The Ocean in the Earth System” and the DFG Priority Program INTERDYNAMIK. The research leading to these results also received funding from the European Union’s Seventh Framework Programme (FP7/2007–2013) under grant agreement 243908, “Past4Future. Climate change–Learning from the past climate.” This is Past4Future contribution n° 69. We thank the Editor and two anonymous reviewers for their constructive remarks on the manuscript.

The Editor thanks two anonymous reviewers for assistance in evaluating this paper.

### References

- Armitage, S. J., S. A. Jasim, A. E. Marks, A. G. Parker, V. I. Usik, and H.-P. Uerpmann (2011), The southern route “out of Africa”: Evidence for an early expansion of modern humans into Arabia, *Science*, *331*, 453–456.
- Bakker, P., et al. (2013), Last Interglacial temperature evolution—A model inter-comparison, *Clim. Past*, *9*, 605–619.
- Braconnot, P., C. Marzin, L. Grégoire, E. Mosquet, and O. Marti (2008), Monsoon response to changes in Earth’s orbital parameters: Comparisons between simulations of the Eemian and of the Holocene, *Clim. Past*, *4*, 281–294.
- Burrough, S. L., and D. S. G. Thomas (2013), Central southern Africa at the time of the African Humid Period: A new analysis of Holocene palaeoenvironmental and palaeoclimate data, *Quat. Sci. Rev.*, *80*, 29–46.
- Castañeda, I. S., S. Mulitza, E. Schefuss, R. A. Lopes dos Santos, J. S. Sinninghe Damsté, and S. Schouten (2009), Wet phases in the Sahara/Sahel region and human migration patterns in North Africa, *Proc. Natl. Acad. Sci. U.S.A.*, *106*, 20,159–20,163.
- Chase, B. M., M. E. Meadows, A. S. Carr, and P. J. Reimer (2010), Evidence for progressive Holocene aridification in southern Africa recorded in Namibian hyrax middens: Implications for African monsoon dynamics and the “African Humid Period,” *Quat. Res.*, *74*, 36–45.
- Claussen, M., S. Bathiany, V. Brovkin, and T. Kleinen (2013), Simulated climate-vegetation interaction in semi-arid regions affected by plant diversity, *Nat. Geosci.*, *6*, 954–958.
- Collins, W. D., et al. (2006), The Community Climate System Model version 3 (CCSM3), *J. Clim.*, *19*, 2122–2143.
- Collins, J. A., et al. (2011), Interhemispheric symmetry of the tropical African rainbelt over the past 23,000 years, *Nat. Geosci.*, *4*, 42–45.
- Collins, J. A., A. Govin, S. Mulitza, D. Heslop, M. Zabel, J. Hartmann, U. Röhl, and G. Wefer (2013), Abrupt shifts of the Sahara–Sahel boundary during Heinrich stadials, *Clim. Past*, *9*, 1181–1191.
- Drake, N. A., R. M. Blench, S. J. Armitage, C. S. Bristow, and K. H. White (2011), Ancient watercourses and biogeography of the Sahara explain the peopling of the desert, *Proc. Natl. Acad. Sci. U.S.A.*, *108*, 458–462.
- Dupont, L. M. (2009), The Congo deep-sea fan as an archive of Quaternary change in Africa and the eastern tropical South Atlantic (a review), in *External Controls on Deep-Water Depositional Systems*, SEPM Special Publication, vol. 92, edited by B. Kneller, O. J. Martinsen, and B. McCaffrey, pp. 79–87, Society for Sedimentary Geology, Tulsa, Okla.
- Engelstaedter, S., I. Tegen, and R. Washington (2006), North African dust emissions and transport, *Earth Sci. Rev.*, *79*, 73–100.
- Gingele, F. X., P. M. Müller, and R. R. Schneider (1998), Orbital forcing of freshwater input in the Zaire Fan area: Clay mineral evidence from the last 200 kyr, *Palaeogeogr. Palaeoclimatol. Palaeoecol.*, *138*, 17–26.
- Govin, A., et al. (2012a), Persistent influence of ice sheet melting on high northern latitude climate during the early Last Interglacial, *Clim. Past*, *8*, 483–507.
- Govin, A., U. Holzwarth, D. Heslop, L. Ford Keeling, M. Zabel, S. Mulitza, J. A. Collins, and C. M. Chiessi (2012b), Distribution of major elements in Atlantic surface sediments ( $36^\circ\text{N}$ – $49^\circ\text{S}$ ): Imprint of terrigenous input and continental weathering, *Geochem. Geophys. Geosyst.*, *13*, Q01013, doi:10.1029/2011GC003785.
- Govin, A., C. M. Chiessi, M. Zabel, A. O. Sawakuchi, D. Heslop, T. Hörner, Y. Zhang, and S. Mulitza (2013), Terrigenous input off northern South America driven by changes in Amazonian climate and the North Brazil Current retroreflection during the last 250 ka, *Clim. Past Discuss.*, *9*, 5855–5898.
- Holtvoeth, J., S. Kolonic, and T. Wagner (2005), Soil organic matter as an important contributor to Late Quaternary sediments of the tropical West African continental margin, *Geochim. Cosmochim. Acta*, *69*, 2031–2041.
- Laskar, J., P. Robutel, F. Joutel, M. Gastineau, A. C. M. Correia, and B. Lestrade (2004), A long-term numerical solution for the insolation quantities of the Earth, *Astron. Astrophys.*, *428*, 261–285.
- Lisiecki, L. E., and M. E. Raymo (2005), A Pliocene–Pleistocene stack of 57 globally distributed benthic  $\delta^{18}\text{O}$  records, *Paleoceanography*, *20*, PA1003, doi:10.1029/2004PA001071.
- Lisiecki, L. E., and M. E. Raymo (2009), Diachronous benthic  $\delta^{18}\text{O}$  responses during late Pleistocene terminations, *Paleoceanography*, *24*, PA3210, doi:10.1029/2009PA001732.
- Lorenz, S. J., and G. Lohmann (2004), Acceleration technique for Milankovitch type forcing in a coupled atmosphere–ocean circulation model: Method and application for the Holocene, *Clim. Dyn.*, *23*, 727–743.
- Loutre, M. F., D. Paillard, F. Vimeux, and E. Cortijo (2004), Does mean annual insolation have the potential to change climate?, *Earth Planet. Sci. Lett.*, *221*, 1–14.
- Maley, J. (1991), The African rain forest vegetation and palaeoenvironments during late quaternary, *Clim. Change*, *19*, 79–98.
- Mulitza, S., M. Prange, J.-B. W. Stuut, M. Zabel, T. von Döbenack, A. C. Itambi, J. Nizou, M. Schulz, and G. Wefer (2008), Sahel megadroughts triggered by glacial slowdowns of Atlantic meridional overturning, *Paleoceanography*, *23*, PA4206, doi:10.1029/2008PA001637.
- Osborne, A. H., D. Vance, E. J. Rohling, N. Barton, M. Rogerson, and N. Fello (2008), A humid corridor across the Sahara for the migration of early modern humans out of Africa 120,000 years ago, *Proc. Natl. Acad. Sci. U.S.A.*, *105*, 16,444–16,447.
- Otto-Bliesner, B. L., R. Tomas, E. C. Brady, C. Ammann, Z. Kothavala, and G. Clauzet (2006), Climate sensitivity of moderate- and low-resolution versions of CCSM3 to preindustrial forcings, *J. Clim.*, *19*, 2567–2583.
- Partridge, T. C., P. B. de Menocal, S. A. Lorentz, M. J. Paiker, and J. C. Vogel (1997), Orbital forcing of climate over South Africa: A 200,000-year rainfall record from the Pretoria Saltpan, *Quat. Sci. Rev.*, *16*, 1125–1133.
- Prell, W. L., and J. E. Kutzbach (1987), Monsoon variability over the past 150,000 years, *J. Geophys. Res.*, *92*, 8411–8425.
- Prospero, J. M., P. Ginoux, O. Torres, S. E. Nicholson, and T. E. Gill (2002), Environmental characterization of global sources of atmospheric soil dust identified with the NIMBUS 7 Total Ozone Mapping Spectrometer (TOMS) absorbing aerosol product, *Rev. Geophys.*, *40*(1), 1002, doi:10.1029/2000RG000095.

- Schefuß, E., H. Kuhlmann, G. Mollenhauer, M. Prange, and J. Pätzold (2011), Forcing of wet phases in southeast Africa over the past 17,000 years, *Nature*, *480*, 509–512.
- Schneider, R. R., B. Price, P. J. Müller, D. Kroon, and I. Alexander (1997), Monsoon related variations in Zaire (Congo) sediment load and influence of fluvial silicate supply on marine productivity in the east equatorial Atlantic during the last 200,000 years, *Paleoceanography*, *12*, 463–481.
- Shackleton, N. J., M. R. Chapman, M. F. Sanchez-Goni, D. Pailler, and Y. Lancelot (2002), The classic marine isotope substage 5e, *Quat. Res.*, *58*, 14–16.
- Street-Perrott, F. A., and R. A. Perrott (1990), Abrupt climate fluctuations in the tropics: The influence of Atlantic Ocean circulation, *Nature*, *343*, 607–612.
- Stuut, J.-B. W., M. Zabel, V. Ratmeyer, P. Helmke, E. Schefuß, G. Lavik, and R. Schneider (2005), Provenance of present-day eolian dust collected off NW Africa, *J. Geophys. Res.*, *110*, D04202, doi:10.1029/2004JD005161.
- Tjallingii, R., M. Claussen, J.-B. W. Stuut, J. Fohlmeister, A. Jahn, T. Bickert, F. Lamy, and U. Rohl (2008), Coherent high- and low-latitude control of the northwest African hydrological balance, *Nat. Geosci.*, *1*, 670–675.
- Tuenter, E., S. L. Weber, F. J. Hilgen, and L. J. Lourens (2003), The response of the African summer monsoon to remote and local forcing due to precession and obliquity, *Global Planet. Change*, *36*, 219–235.
- Varma, V., M. Prange, U. Merkel, T. Kleinen, G. Lohmann, M. Pfeiffer, H. Renssen, A. Wagner, S. Wagner, and M. Schulz (2012), Holocene evolution of the Southern Hemisphere westerly winds in transient simulations with global climate models, *Clim. Past*, *8*, 391–402.
- von Storch, H., and F. W. Zwiers (1999), *Statistical Analysis in Climate Research*, 494 pp., Cambridge Univ. Press, Cambridge, U. K.
- Walter, R. C., et al. (2000), Early human occupation of the Red Sea coast of Eritrea during the Last Interglacial, *Nature*, *405*, 65–69.
- Weltje, G. J., and R. Tjallingii (2008), Calibration of XRF core scanners for quantitative geochemical logging of sediment cores: Theory and application, *Earth Planet. Sci. Lett.*, *274*, 423–438.
- Yeager, S. G., C. A. Shields, W. G. Large, and J. J. Hack (2006), The low-resolution CCSM3, *J. Clim.*, *19*, 2545–2566.